World Academy of Science, Engineering and Technology
International Journal of Mechanical and Industrial Engineering
Vol:17, No:10, 2023

Investigation of Gas Tungsten Arc Welding Parameters on Residual Stress of Heat Affected Zone in Inconel X750 Super Alloy Welding Using Finite Element Method

Kimia Khoshdel Vajari, Saber Saffar

***Abstract*—**Reducing the residual stresses caused by welding is desirable for the industry. The effect of welding sequence, as well as the effect of yield stress on the number of residual stresses generated in Inconel X750 superalloy sheets and beams, have been investigated. The finite element model used in this research is a three-dimensional thermal and mechanical model, and the type of analysis is indirect coupling. This analysis is done in two stages. First, thermal analysis is performed, and then the thermal changes of the first analysis are used as the applied load in the second analysis. ABAQUS has been used for modeling, and the Dflux subroutine has been used in the Fortran programming environment to move the arc and the molten pool. The results of this study show that the amount of tensile residual stress in symmetric, discontinuous, and symmetric-discontinuous welds is reduced to a maximum of 27%, 54%, and 37% compared to direct welding, respectively. The results also show that the amount of residual stresses created by welding increases linearly with increasing yield stress with a slope of 40%.

***Keywords*—**Residual stress, X750 superalloy, finite element, welding, thermal analysis.

I. Introduction

RESIDUAL welding stresses are a key parameter which needs to be controlled in order to minimize failures at the weld site. Welding residual stresses are caused by differential thermal expansion and contraction of the weld metal and parent material. This stress is the internal stress that remains in a material after the external forces that caused it are removed. Residual stress can affect the performance, quality, and durability of welded components, as well as increase the risk of distortion, cracking, and failure. Therefore, it is important to understand how residual stress is generated in welding and how it can be reduced or eliminated. Therefore, for industrial reasons, the nature of residual stresses due to welding should be understood and predicted and their relationship with different process conditions and material behavior should be determined. Due to the importance of residual stress in various industries such as marine, military and petrochemical industries, it is necessary to conduct more studies in this regard. Studies to investigate residual stresses due to welding are very extensive. In the past, studies have been conducted with the aim of reducing residual stresses resulting from welding, for example, methods including sequential welding [1]-[5], heat and mechanical treatment [6]-[10], and new techniques in the welding process [11]-[15] have been studied and evaluated to reduce residual stresses. Since residual stresses are caused by local heating and local contractions and expansions during welding, in most cases it is recommended to take measures to control and minimize them, if possible, during welding. Control of welding conditions such as inlet heat by controlling restraints and using different welding techniques are in this category. But methods to reduce residual stresses after welding are also considered. These methods are based on the principle of plastic deformation in welded parts to reduce residual stresses. Recently, in 2014, Zubairuddin et al. [16] investigated the residual stress and distortion caused by 3 mm thick 9Cr-1Mo steel plates during GTA welding.

In this study, SYSWELD software was used for thermal analysis. A three-dimensional mesh model has been developed for the simulation, using a dual elliptical heat source distribution for thermal analysis. In this study, comparison of experimental and numerical results has shown that if the theory of large distortion is used, the accuracy of numerical results will be higher. Faraji et al. [17] used pure commercial aluminum in a 2D numerical model to predict the shape of the weld pool in fixed gas tungsten arc (GTA) welding, regardless of the fluid flow in the weld pool. In this study, the Gaussian flow current density and the input heat distribution on the workpiece surface were considered. The results of this study show that the distribution parameters are functions of current and arc length. Therefore, the effects of arc length, flow and welding time on the geometry of the welding pool were investigated. In 2015, Liu et al. [18] investigated complex transition phenomena and their effects on welding pool dynamics and surface ripple in gas tungsten arc welding (GTAW) under pulsed currents using a three-dimensional transient numerical model. In this study, the flow velocity and temperature distribution of the flow and the formation of the weld bead are simulated. The results show that for medium current cases, pulsed current leads to deeper weld penetration than continuous current. Larger pulse frequency

Kimia Khoshdel Vajari is with Faculty of Engineering, Islamic Azad University-Tehran North Branch, Sadoughi Blvd, Hakimiyeh Wayout, Shahid Babaei Highway, Tehran, 1651153311, Iran.

Saber Saffar is with Faculty of Petroleum Engineering, Amirkabir University of Technology (Tehran Polytechnic), Tehran, Iran, P.O. Box 1591634311, Tehran, I.R. Iran (corresponding author, e-mail: s.saffar@aut.ac.ir)

also leads to a more uniform distribution of thermal energy on the workpiece and tends to reduce the solidification rate, thus leading to a more uniform penetration depth, smaller surface area and wave height. In the study by Bahrami et al. [19] in 2015, the transition processes related to the mixing of two different alloys in the GTAW pool are investigated numerically and experimentally. The numerical model includes electromagnetic fields, velocity, temperature and concentration. This model is completely solved using COMSOL Multiphysics software.

In 2016, Vankatkumar and Ravindran [20] studied the distortion caused by the AISI 304 SS rectangular plate during the GTA welding process, which is experimentally measured and mostly verified using finite element analysis (FE). In this study, the thermal history is measured at fixed points on the surface of the plate and the results are compared with FE analysis. Zubairuddin et al. [21] in 2017, studied the thermal-mechanical analysis of GTA welding of several passes of steel plate with a thickness of 6 mm; 91 using three different models including a two-dimensional model, a large three-dimensional lattice model and a three-dimensional mesh model is fine-tuned. Predicted thermal cycles, residual stress and distortion were confirmed using experimental instruments. The effect of preheating between welding passes on simulated distortion was also experimentally confirmed. In 2017, Magalhães et al. [22] present an analysis of the thermal effect of heat transfer by convection and radiation during the GTA welding process. Modified from an internal C^{++} code to calculate the amount of heat transfer by convection and radiation. In this software, an iterative Broydon-Fletcher-Goldfarb-Shanno (BFGS) inverse method was used to estimate the amount of heat delivered to the plate when determining the appropriate sensitivity criteria. This study showed that heat loss due to displacement and radiation of the boiling pool has no effect on the cooling process.

In 2018, Huang et al. [23] discussed the mechanism of porosity formation from a chemical, physical, and metallurgical perspective. Considering that the welding current has a significant effect on the porosity defect, the effect of the welding current on the critical core radius was investigated. The results showed that the critical core radius is the same in the two models, which is slightly affected by the welding current. This means that flow plays an important role in the bubble growth stage. Wang et al. [24] in 2019 aimed to understand the heat transfer and fluid flow of the plasma arc and the welding pool by significantly deforming the surface of the welding pool during high GTAW. In this study, a single model including tungsten electrode, plasma arc and welding pool of low carbon steel is developed by determining a free surface deformation from experimental observations. The buoyancy, Lorentz force, plasma tensile force and Marangoni force are considered to study the dynamics of the weld pool with high depressed free surface. In 2020, Xu et al. [25] studied the distance between the tungsten electrode tip and laser beam axis (DLa) on the key energy transfer behavior during hybrid welding with titanium arc laser. They used energy analysis methods to analyze the next parameters and welding efficiency. A "sandwich" structure consisting of a glass plate and titanium alloy is used to directly monitor the physical properties of the composite arc and laser cap. Using spectral detection method, combined plasma coupling discharge modes under different Dla were investigated. In 2020, Shirvastava et al. [26] investigated the effect of process parameters on weld distortion and weld penetration depth in GTA welded stainless steel plate made of AISI 304 stainless steel. The main goal of the process variable is to achieve the minimum weld distortion and the maximum weld nut penetration or penetration depth. Four welding currents of inlet parameter, gas flow velocity, face root and welding velocity were selected to determine their effect on distortion and penetration depth. The results showed that the welding speed (WS) is the most important parameter for distortion during GTA welding. In the present study, the effect of parameters such as linear velocity and electrode diameter on the amount of residual stress in the heat affected zone in this type of alloy is investigated.

II. Theory

In the finite element method, there are two distinct approaches for thermodynamic analysis: direct method (coupled) and indirect method (non-coupled). The direct method consists of only one analysis. In finite element analysis, the coupled method uses elements that have all the degrees of freedom required for analysis. In this method, matrices of elements and force vectors include all the required terms. In the non-coupled method, the analysis is performed in two stages. In modeling the welding process, three areas of heat transfer, metallurgical and mechanical are interrelated that the choice of the appropriate analysis method for welding analysis depends on how these three areas are related. Uneven distribution of heat causes stress in the part. The finite element model used in the present study is a three-dimensional thermal and mechanical model and the type of analysis is indirect coupling. This analysis is performed in two stages, in first stage, thermal analysis is performed and in the second stage, the thermal variation is studied. The first analysis is used as the applied load in the second analysis. ABAQUS finite element software is used for modeling. Figs. 1 and 2 show the thermal and mechanical boundary conditions considered in the model geometry and welding method. The sample includes a sheet with dimensions of 300 mm × 200 mm × 5 mm on which single-stage welding is performed.

A. Thermal Modeling

Simulation of heat transfer problems is the first step in analyzing welding problems. At this stage, the temperature of the model nodes is calculated by defining the initial thermal conditions as well as the boundary conditions and using the fundamental relations of transient heat transfer. The thermal properties of materials are also commonly known as thermophysical properties and include two distinct categories of transfer properties and thermodynamic properties. Transfer properties include thermal conductivity k (in heat transfer) and kinematic viscosity v (in motion transfer). Thermodynamics defines the state of the system. Density p and specific heat c are two thermodynamic properties that are widely used in

thermodynamic analysis. The product of ρ.cp, usually called volumetric heat capacity, expresses the ability of matter to store heat energy. In heat transfer analysis, the ratio of thermal conductivity to heat capacity is called heat dissipation coefficient and is expressed in m^2s^{-1}.

$$\alpha = \frac{k}{\rho c_p} \quad (1)$$

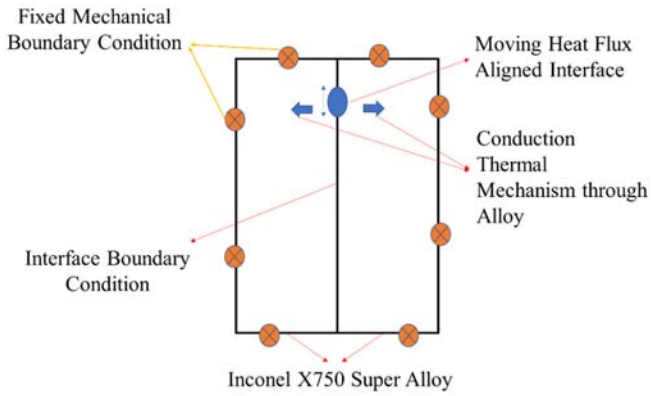

Fig. 1 Thermal and mechanical boundary conditions of the problem

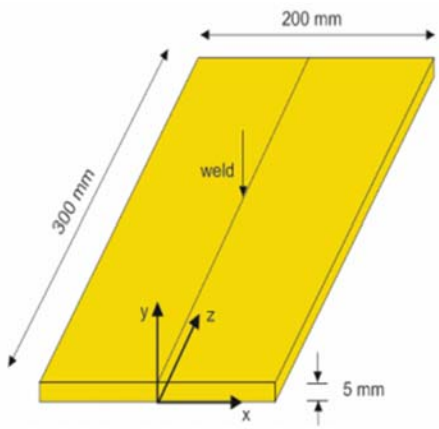

Fig. 2 Geometric dimensions of the problem and the direction of the coordinate axes

Welding is a time-dependent process and therefore the transient heat transfer equation should be used in its thermal study. When a volume is surrounded by plates in six sides of an element, the thermal equilibrium is expressed by:

$$\frac{\partial}{\partial X}\left(K_X \frac{\partial T}{\partial X}\right) + \frac{\partial}{\partial Z}\left(K_Y \frac{\partial T}{\partial Y}\right) + \frac{\partial}{\partial Z}\left(K_Z \frac{\partial T}{\partial Z}\right) + Q = \rho C \frac{\partial T}{\partial t} \quad (2)$$

In this equation, T is the current temperature at any moment Q is the rate of initial heat production and t is time. Also, K_X, K_Y and K_Z are the thermal conductivity coefficients in the X, Y and Z directions, respectively. The welding energy with the heat that enters the part from the electric arc is obtained from:

$$Q_W = \eta . V . I \quad (3)$$

In this equation η is the efficiency of the arc. V is the welding voltage and *I* is the welding current intensity. The model used in this research is a three-dimensional heat source model developed by Teng and Lin [27]. This model is based on observations from the molten region and therefore compared to other models presented to date. They have a higher accuracy and flexibility. This model has an elliptical structure and for this reason it is also referred to as a double elliptical model. This model is a combination of two different ellipses, one in the front quarter of the heat source and the other in the rear quarter. C_1, C_2, B and *a* are constant parameter which can determine how the heat source is distributed. In the physical state, these parameters are the radial dimensions of the molten area in front, back, side and under the arch [3]. The heat source model used in this research is a three-dimensional heat source model called the double elliptical model, which is presented in detail in reference [27] and is shown in Fig. 3. Heat source energy densities, which express how heat flux is distributed within the front and rear quarters, can be expressed by (4) and (5):

$$q_f(x.y.z) = \frac{6\sqrt{3} f_f Q}{abc_f \pi\sqrt{\pi}} . e^{-3\frac{x^2}{a^2}} . e^{-3\frac{x^2}{b^2}} . e^{-3\frac{x^2}{c_f{}^2}} \quad (4)$$

$$q_r(x.y.z) = \frac{6\sqrt{3} f_{fr} Q}{abc_r \pi\sqrt{\pi}} . e^{-3\frac{x^2}{a^2}} . e^{-3\frac{x^2}{b^2}} . e^{-3\frac{x^2}{c_r{}^2}} \quad (5)$$

These equations represent the input energy which is determined based on (6) by the welding current, welding voltage and efficiency of the welding technology used.

$$Q = I \times V \times \eta \quad (6)$$

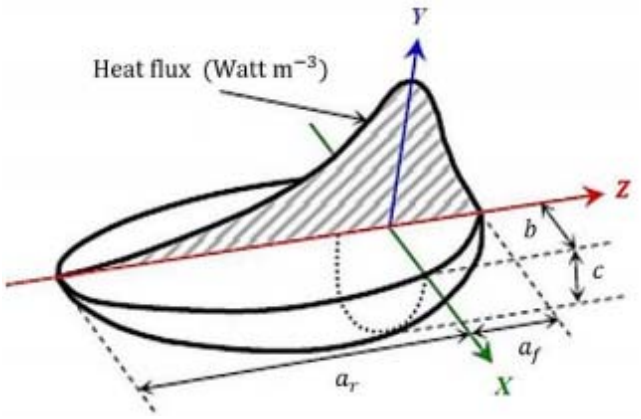

Fig. 3 Cross-sectional dimensions of two elliptical heat sources

Sediment heat fraction factors can be obtained from (7)-(9):

$$f_f = \frac{2C_f}{C_f + C_r} \quad (7)$$

$$f_r = \frac{2C_r}{C_f + C_r} \quad (8)$$

$$f_f + f_r = 2 \quad (9)$$

The coefficient of thermal conductivity of the melting zone

was doubled to simulate the infiltration of the weld pool [14]. The latent heat of melting is considered to model the thermal effects of freezing in the boiling pool. Thermal enthalpy method was used to use latent heat in finite element simulation analysis. The German type used for thermal modeling has three-dimensional thermal conductivity. This element has eight nodes, each node has a degree of freedom (temperature) and the properties of the same material.

B. Mechanical Modeling

Mechanical analysis of the welding process has higher variables and nonlinear degrees than thermal analysis. In mechanical analysis, the temperature history obtained from thermal analysis is entered into the mechanical analytical equations as thermal load, thermal stress and strain are calculated at each time step, and the final state of residual stress is created by the accumulation of thermal stresses and strains. This is done in such a way that mechanical stresses are obtained during each time by applying the heat distribution obtained from thermal analysis.

Existence of high temperature changes during the welding process causes non-linear behavior of the material. Mechanical properties include Young's modulus {E}, Poisson's ratio {v}, Yield stress $\{\sigma_Y\}$, and the coefficient of thermal expansion {α}, which are effective in the thermoelastic and thermoplastic analysis of the welding process. The main equations for mechanical analysis include equilibrium equations and basic equations.

$$\partial_{ij} + Pb_{ij} = 0 \quad (10)$$

$$\sigma_{ij} = \partial_{ji} \quad (11)$$

where σ_{ij} is the stress tensor and the volumetric force b_i. Equation (11) shows the symmetry of the stress tensor.

$$[d\sigma] = [D^{ep}][d\varepsilon] - [c^{th}]dT \quad (12)$$

$$[D^{ep}] = [D^{e}] + [D^{p}] \quad (13)$$

In these equations, $[D^e]$ is the elastic stiffness matrix, $[D^p]$ is the plastic stiffness matrix, $[c^{th}]$ is the thermal stiffness matrix dσ except stress, dε except strain and dT except temperature.

III. FEM Modeling

In order to consider the effect of material microstructure, 20-node quadratic brick elements (type C3D20R) were utilized. The analysis accounts for the geometric non-linearity associated with large deformation. Preliminary analysis showed that the differences in the results obtained from linear and non-linear simulations are sufficiently large to indicate that a linear simulation is not adequate for these welding simulations. For all cases, very fine hexagonal type mesh is utilized in welding area. A typical mesh used welding line considering is shown in Fig. 4. As is clear in the figure, the half of the plate (welding line is the symmetry line) is modeled due to the symmetry. Also, for all cases, 19392 solid elements were considered.

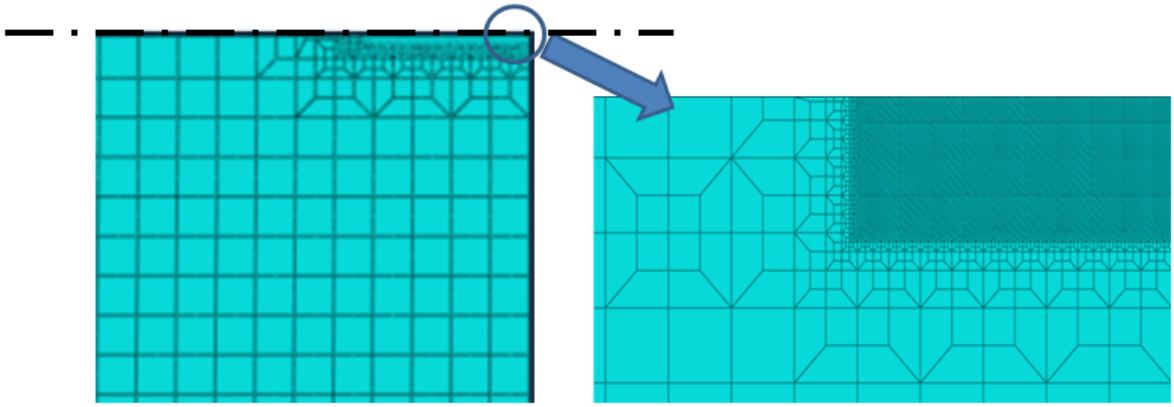

Fig. 4 Mesh modeling proposed to welding simulation

Also, in order to move the electric arc and the molten pool, Dflux subroutine has been used in the FORTRAN programming environment. The type of elements in both thermal and mechanical analysis is eight nodes. The parameters required for welding are also shown in Table I. It should be noted that the properties of materials such as Young's modulus, yield stress, Poisson ratio, heat transfer coefficient, specific heat capacity and longitudinal expansion coefficient are considered as variables due to high temperature changes.

TABLE I
WELDING PARAMETERS

Speed	Arc efficiency	Voltage	Ampere
5 mm	0.7	20	110

During welding, the properties of materials change with increasing temperature. In Table II, the properties of materials including Young's modulus, yield stress, Poisson ratio, and heat transfer coefficient, specific heat capacity and longitudinal expansion coefficient according to the temperature changes are given.

TABLE II
MECHANICAL PROPERTIES OF USED MATERIAL AT DIFFERENT TEMPERATURES

Properties	Temperature									
	0	200	400	500	600	700	800	1200	1600	2000
Young's modulus (GPa)	209	160	120	70	40	15	15	15	15	15
Yield stress (MPa)	160	160	160	100	20	15	15	15	15	15
Poisson's ratio	0.29	0.295	0.3	0.305	0.31	0.32	0.32	0.32	0.32	0.32
Termal conductivity (W/mc)	59	51	42	38	35	32	32	32	32	32
Specific heat (j/kg c)	45	60	100	122	130	140	140	140	140	140
Coefficient of thermal expansion (x10E-5)	1.2	1.25	1.3	1.4	1.45	1.5	1.5	1.5	1.5	1.5

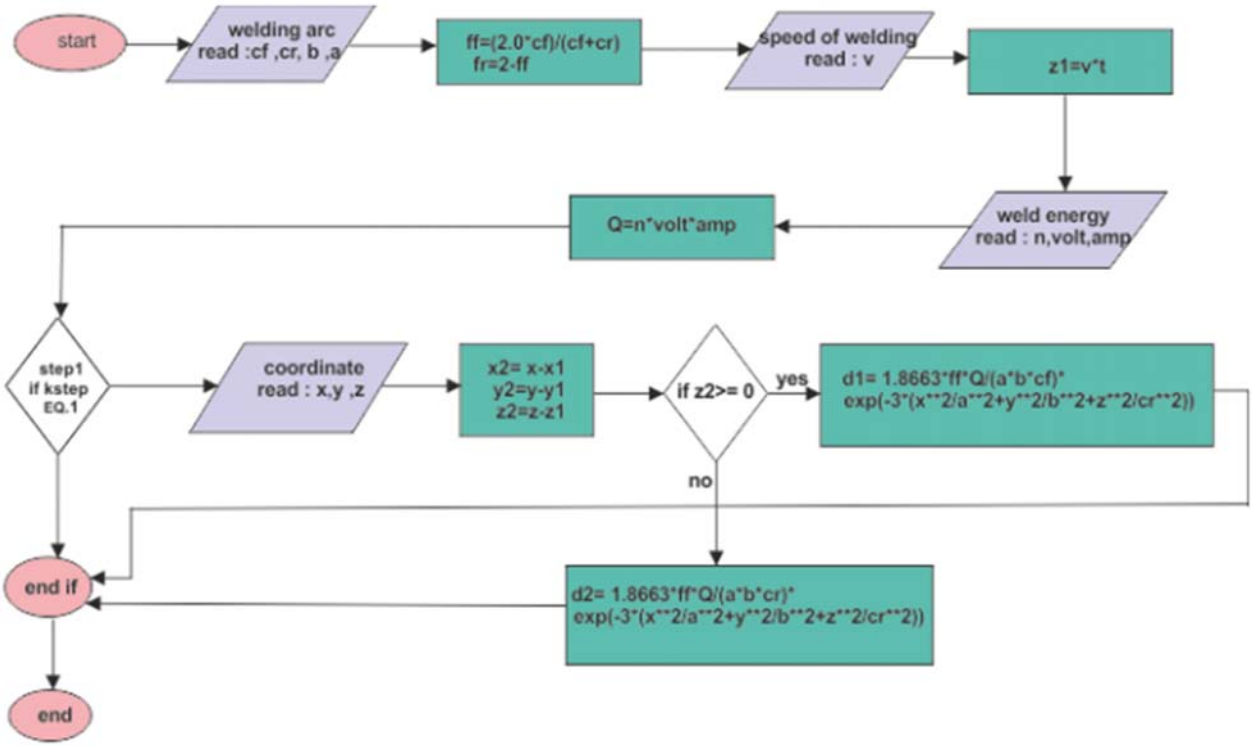

Fig. 5 Subroutine algorithm for one step of welding

Fig. 5 shows the subroutine algorithm for one step of welding. In this algorithm, first the arc parameters including cf, cr, b, and a are introduced to the Fortran program, then with the ff and fr operators, the amount of weld deposition is calculated according to the input data. Then, the WS is given to the program and the welding length is obtained according to the elapsed time. After entering the WS, the data required for welding energy are given to the program, which include amps, voltage and efficiency. These values are then multiplied by each other. After entering the initial data, the steps are introduced to the program according to the number of paths or welding steps. The algorithm in Fig. 5 has one step. Then, the welding coordinates and the direction in which the welding will be done are introduced to the program. After being welded for welding, it is the turn of the welding melt pool, which according to the formulas presented in the previous section, enters the conditional part of the algorithm.

A. Investigation of the Effect of Weld Motion Direction on Residual Stress

After evaluating the accuracy of the finite element model, the effect of welding sequence and type of welder movement on residual stresses was investigated. For this purpose, four models have been studied, which are welding motion in direct mode, welding motion in discontinuous mode, welding motion in symmetric mode and welding motion in symmetrical-discontinuous mode. In direct welding mode, a welding step is used. In the symmetrical welding mode, two opposite welding movements are used in the same direction, and in the intermittent and discontinuous-symmetric welding mode, four welding steps are used. Fig. 6 shows how to move the welding line in the studied cases.

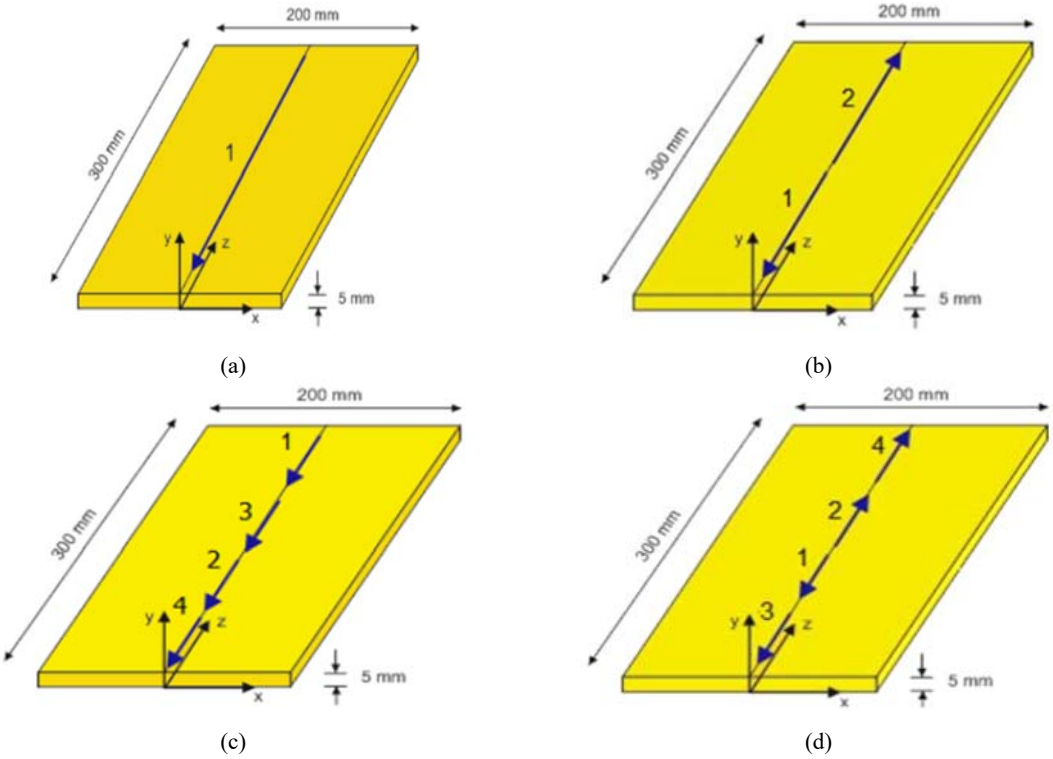

Fig. 6 (a) How to move the weld in a straight state, (b) How to move the weld in a symmetrical state, (c) How to move a weld in a discontinuous state, (d) How to move a weld in a discontinuous-symmetrical state

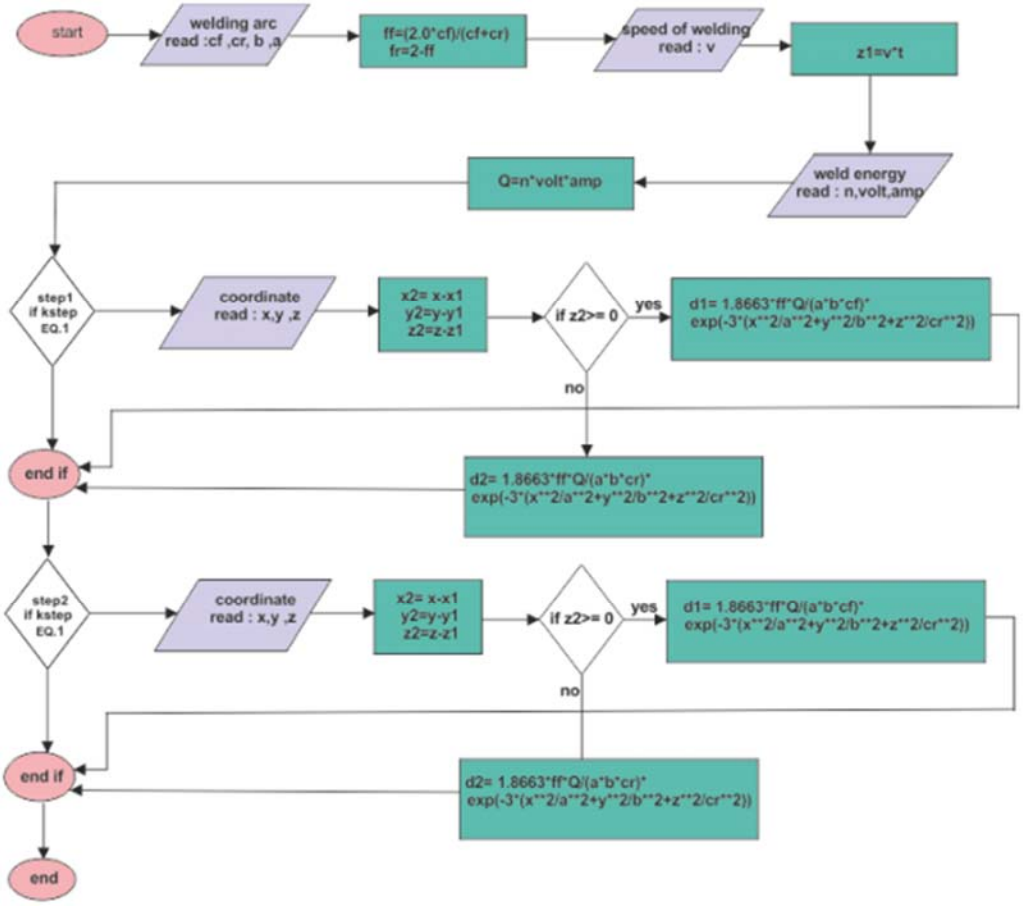

Fig. 7 Subroutine algorithm in synchronous mode with two steps

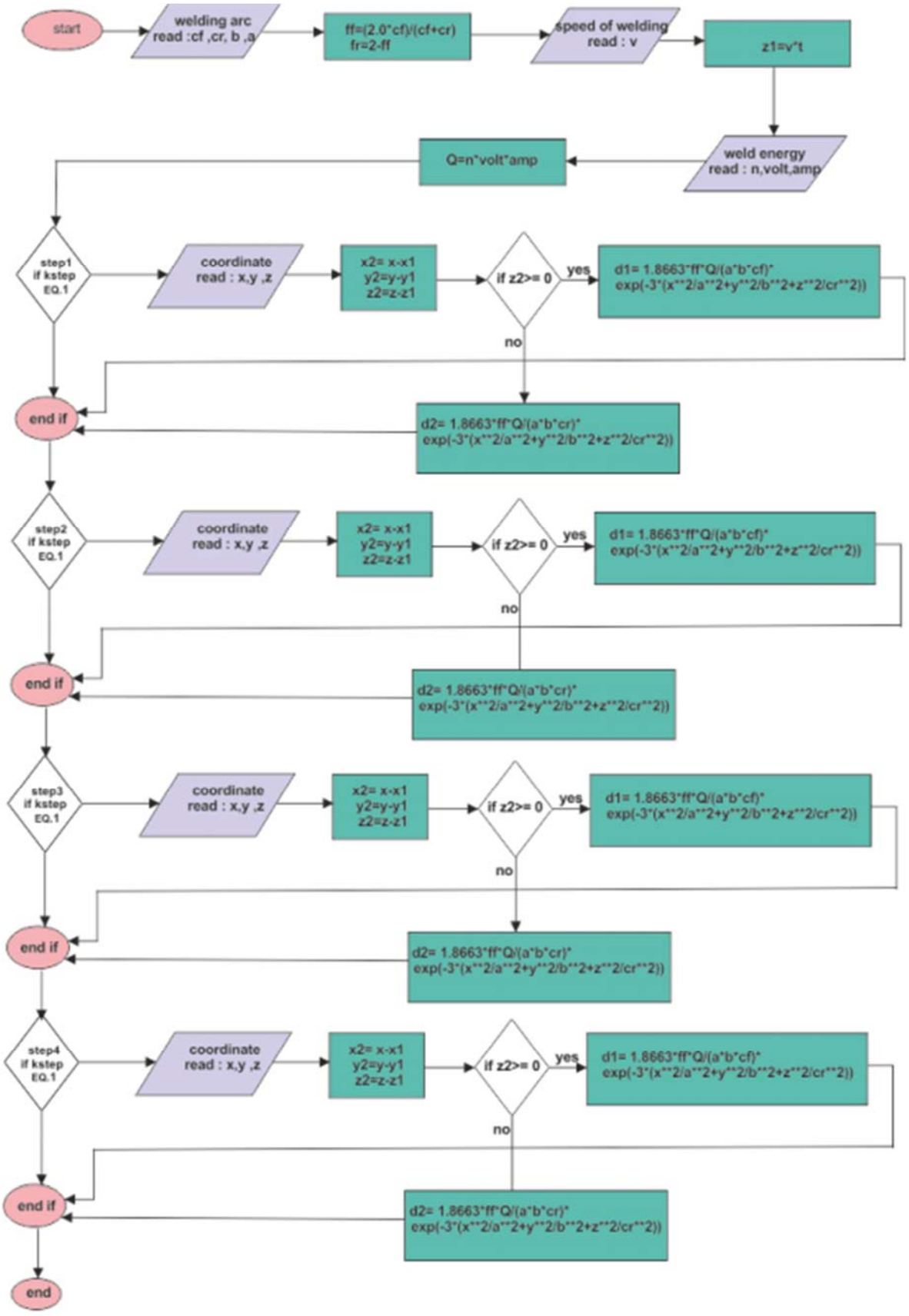

Fig. 8 Algorithm for four-step discontinuous subroutine

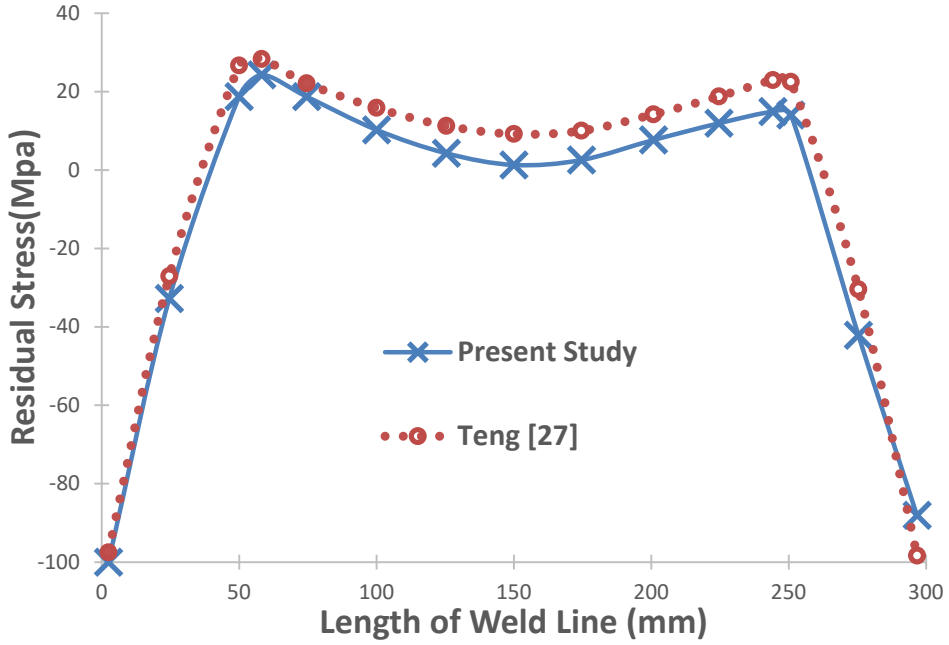

Fig. 9 Comparison of residual stresses from the present numerical solution and Teng [27] model for validation

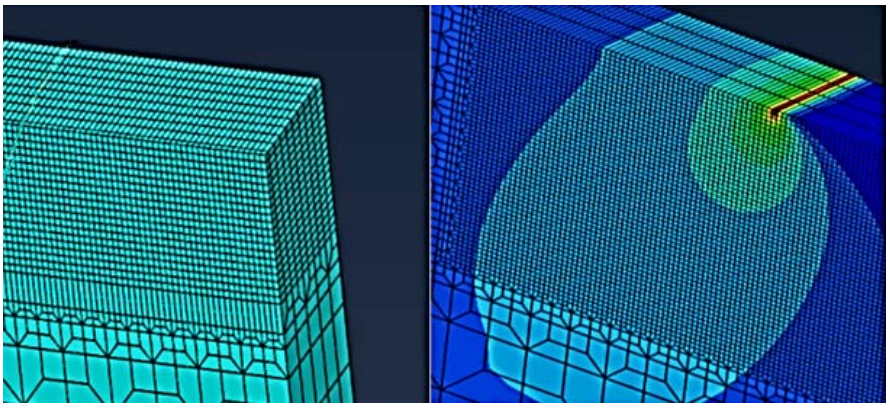

Fig. 10 A schematic of stress distribution around the heat source

Fig. 6 (b) shows how the weld line moves in a symmetrical state. In this model, two welding lines are used, which start welding in a symmetrical position from the middle of the plate. Fig. 7 shows the subroutine algorithm for two steps of welding for the symmetrical welding mode. In this algorithm, like the algorithm described in Fig. 5, first, the arc parameters including cf, cr, a, b are introduced to the Fortran program, then the WS is given to the program. After entering the WS, the data required for welding energy are given to the program, including amps, voltage and efficiency. Then, these values are multiplied by each other. Due to the movement that exists in the symmetric state, two welding steps are used. Also, Figs. 6 (c) and (d) show intermittent welding and Fig. 8 shows the subroutine algorithm for intermittent welding.

IV. Results

A. Validation

The validation results between the studied model and Teng's model are shown in Fig. 9. In order to calibrate the numerical solution performed in this study, a three-dimensional simulation of the problem solved in Teng's model [27] has been performed. The waste generated in the workpiece is addressed. According to the comparison, the amount of residual stress in the compressive state in the maximum state in the Teng model [27] was equal to 100 MPa, which in the case of studies is 95 MPa at the beginning of the sheet and 90 MPa at the end of the sheet. Also, the maximum amount of tensile residual stress in the Teng model in the first third of the sheet is equal to 27 MPa, in the middle of the sheet is equal to 10 MPa, and in the last third of the sheet is equal to 25 MPa. It is almost the same for the presented model. As shown in Fig. 9, the residual stress is equal to 25 MPa in the first third of the sheet, and in the middle of the sheet is equal to 5 MPa, and in the last third of the sheet is equal to 15 MPa.

Therefore, the case study of compressive residual stress at the beginning of the sheet is 5% and the tensile residual stress

at the beginning of the sheet in the study model is 7% different from the narrow model. In general, there are slight differences. Therefore, it is possible to use this FEM model in the rest of the simulations. An example of the simulation to show the pattern of stresses distribution induced by heat source is shown in Fig. 10.

B. Comparison of Longitudinal Residual Stresses in Different Welding Motion States

Fig. 11 shows the residual stresses caused by welding in four states (straight, symmetrical, discontinuous and discontinuous-symmetric).

The study of welding motion in Inconel X750 superalloy plates has shown that the amount of residual stress in the symmetrical, discontinuous and symmetrical-discontinuous states has been significantly reduced compared to direct welding. The effect of this reduction in the intermittent state was greater than in other states. On the other hand, due to the fact that the presence of residual stresses may cause premature rupture in welding areas, so it reduces the choice of welding and increases the reliability of welding operations. The reason for the higher residual stress in the direct welding mode may be that the heat generated during welding is due to the non-stop welding effect and due to the poor heat transfer of Inconel metal; it causes a high temperature gradient. This temperature gradient can generate more residual stress during cooling. But as the number of welding passes increases, the chance of heat transfer increases, which helps to create a lower temperature gradient in intermittent welding. Lower temperature gradients also reduce residual stress.

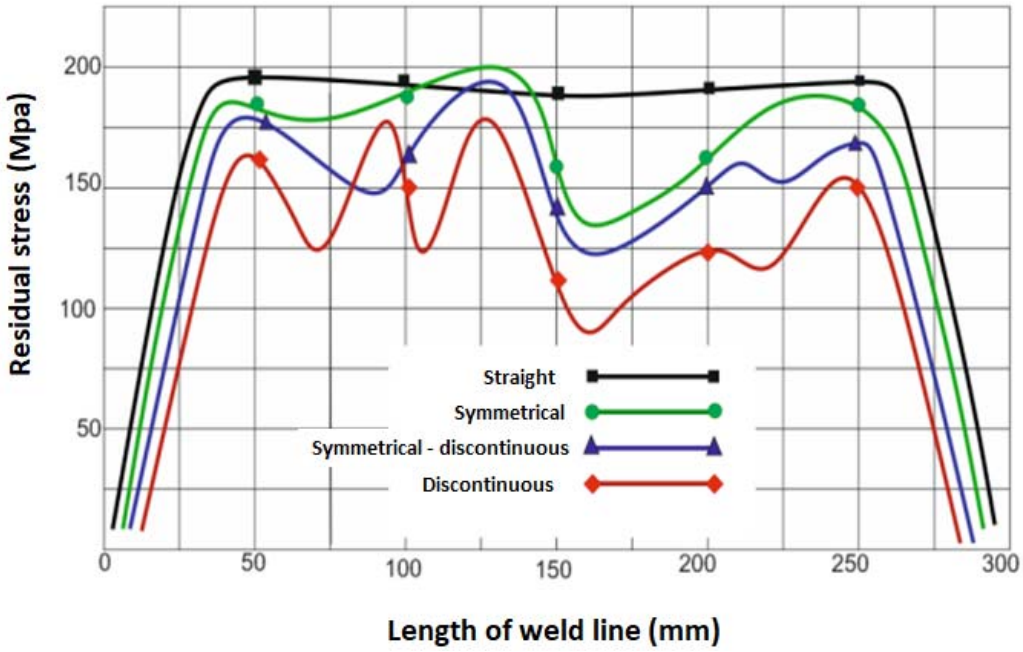

Fig. 11 Comparison of residual stresses in four-state mode

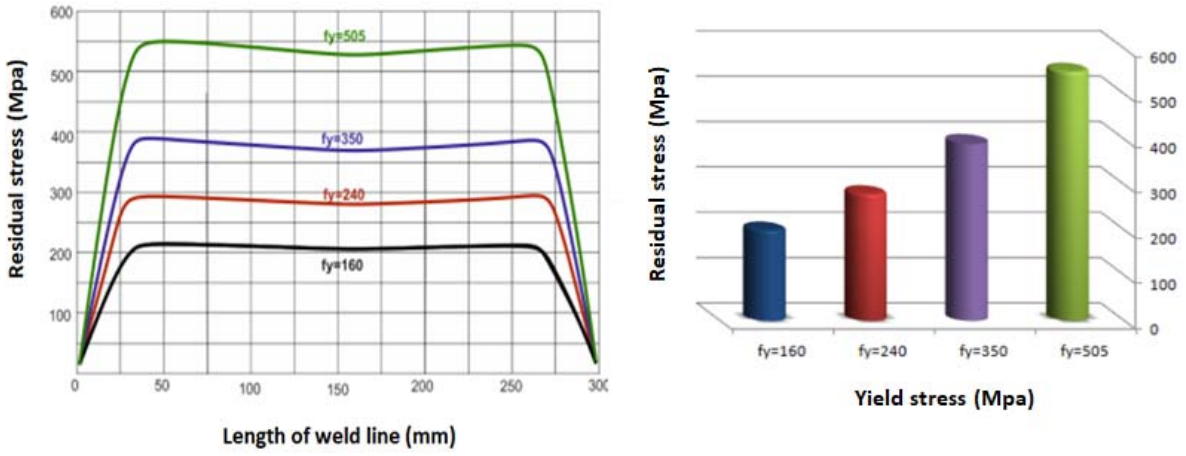

Fig. 12 Longitudinal residual stress

C. Investigation of the Effect of Yield Stress on Residual Stress

In order to investigate the effect of yield stress on residual stresses caused by Joss, four models with different yield stresses have been investigated. In this study, welding current of 110 amps, welding voltage of 20 volts and arc efficiency of 0.7 and its speed of 5 mm per second are considered.

Fig. 12 shows the longitudinal residual stresses. It is clear that with increasing yield stress, the amount of tensile residual stresses has increased linearly. The reason for the increase in residual stress with increasing yield stress of the base metal can be due to the increase in the strength of the base metal and as a result its greater resistance to deformation. This resistance to deformation manifests itself as residual stresses within the part.

Also, Fig. 13 shows the transverse residual stresses. In this figure, too, with increasing yield stress, the amount of compressive residual stresses has increased.

According to Figs. 12 and 13 related to the longitudinal and transverse residual stresses, it can be understood that yield stress has a significant effect on the amount of residual stresses created in welded joints. This rate increases linearly with increasing yield stress.

V. Conclusion

In this study, the effect of welding motion and its effect on residual stress and the effect of yield stress on residual stresses caused by welding were investigated. The present study has shown that with the help of finite element method for three-dimensional thermo-plastic simulation of the welding process, temperature gradient, residual stress field and deformation in different parts of a weld joint can be obtained and the effect of changing different parameters for connection optimization has also been investigated. Also, the present study has shown that by performing proper simulation, the costs of trial and error to design a good connection can be avoided.

- Study on welding motion in Inconel X750 super alloy sheets has shown that the amount of residual stress in the tensile state in the symmetric, discontinuous and symmetric-discontinuous states in the maximum state of 27%, 54% and 37%, respectively. They have a reduction compared to direct welding. Also, the rate of reduction in the intermittent state was greater than other states. On the other hand, due to the presence of residual stresses that may cause premature rupture in the welding areas, so the choice of intermittent welding reduces the risk of welding and reliability of welding operations increasing. Therefore, in carrying out appropriate designs of connections, this point must be considered.
- The results showed that the yield stress has a significant effect on the amount of residual stresses caused by welding in the sheet under study that this rate increases linearly with increasing yield stress with a slope of 40%.

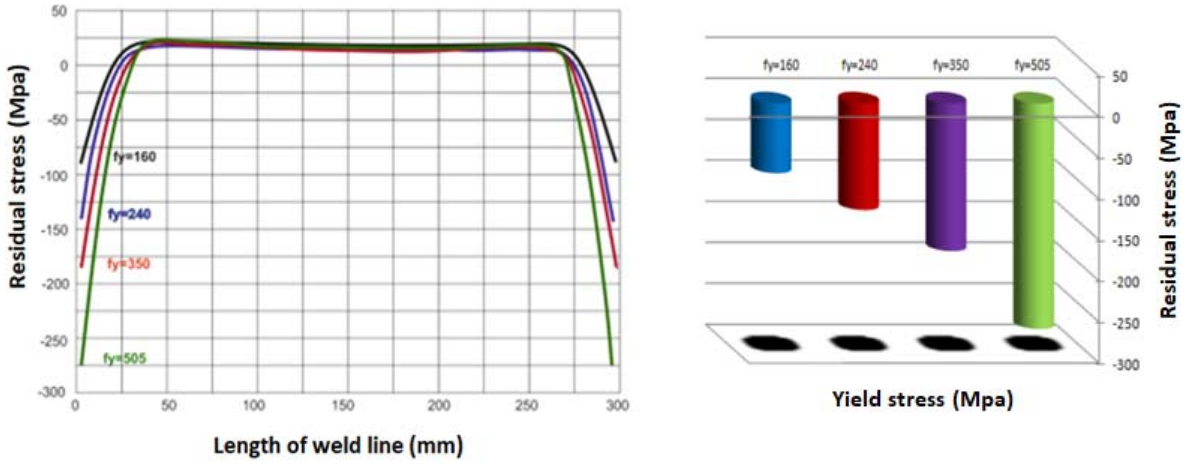

Fig. 13 Transverse residual stress

References

[1] Feng Z, Processes and Mechanisms of Welding Residual Stress and Distortion, Woodhead Publishing in Materials, 1th Edition, 2005.
[2] Zinn W and Scholtes B, "Residual Stress Formation Processes During Welding and Joining", ASM International, pp.391-396, 2002.
[3] Masubuchi k, Analysis of Welded Structures, Pergamon Press, 1th Edition, 1980.
[4] Nitschke T, Wohlfahrt H, "Residual Stresses in Welded Joints", European Conference on Residual Stresses, 2002.
[5] Cary H.B and Helzer S.C, Modern Welding Technology, Pearson Prentice Hall, 6th Edition, pp. 609-611, 2005.
[6] Engelhard M, Pellkofer D, Schmidt J and Weber J, "Optimization of Residual Welding Stresses in Austenitic Steel Piping: Proof Testing and Numerical Simulation of Welding and Postwelding Processes", Nuclear Engineering and Design, Vol.198, pp.141-151, 2000.
[7] Miyazaki k, Numata M, Saito k and Mochizuki M, "The Effect of the Distance from the Center of a Weld to the Fixed End on the Residual Stress and Stress Intensity Factor of a Piping Weld", ASME Pressure Vessels and Piping Division Conference, Colorado USA, 2005.
[8] Lindgren M, Lepisto T, "Vibratory Stress Reliving Treatment of Welded Steel", European Conference on Residual Stresses, 2002.
[9] Lohe D and Vohvinger O, "Stability of Residual Stresses", ASM International, pp.54-69, 2002.
[10] Cho J.R, Lee B.Y, Moon Y.H and Van Tyne C.J, "Investigation of Residual Stress and post Weld Heat Treatment of Multi Pass Welds by Finite Element Method and Experiments", Journal of Materials Processing Technology, Vol.155, pp. 1690-1695, 2004.
[11] Hauk V, Hougardy H and Macherauch E, "Residual Stresses Measurement Calculation, Evaluation, "DGM Information Gesellshaft, Germany, pp.121-135, 1991.
[12] West S.L, "Modeling of Residual Stress Mitigation in Austenitic Stainless Steel Pipe Girth Weldment", International Conference on Modeling and

Control of Joining Processes, 1993.
[13] Bruno G, "Residual Stress Microstructural Changes Induced by Welding in Materials for Nuclear Technology", ISIS Experimental Report, 1998.
[14] Fricke S, Keim E and Shmidt J", Numerical Weld Modeling a Method for Calculation Weld Induced Residual Stresses", Nuclear Engineering and Design, Vol.206, pp.139-150, 2001.
[15] Saperstein Z.P, Control of Distortion and Residual Stress in Weldments, American Society for Metals, 2th Edition, 1977.
[16] Zubairuddin, Mohammed, et al. "Experimental and finite element analysis of residual stress and distortion in GTA welding of modified 9Cr-1Mo steel." *Journal of Mechanical Science and Technology* 28.12 (2014): 5095-5105.
[17] Faraji, A. H., et al. "Numerical and experimental investigations of weld pool geometry in GTA welding of pure aluminum." *Journal of Central South University* 21.1 (2014): 20-26.
[18] Liu, J. W., et al. "Numerical investigation of weld pool behaviors and ripple formation for a moving GTA welding under pulsed currents." *International Journal of Heat and Mass Transfer* 91 (2015): 990-1000.
[19] Bahrami, Alireza, et al. "Study of mass transport in autogenous GTA welding of dissimilar metals." *International Journal of Heat and Mass Transfer* 85 (2015): 41-53.
[20] Venkatkumar, D., and D. Ravindran. "3D finite element simulation of temperature distribution, residual stress and distortion on 304 stainless steel plates using GTA welding." Journal of Mechanical Science and Technology 30.1 (2016): 67-76.
[21] Zubairuddin, M., et al. "Numerical simulation of multi-pass GTA welding of grade 91 steel." *Journal of Manufacturing Processes* 27 (2017): 87-97.
[22] Magalhaes, Elisan Dos Santos, Ana Lúcia Fernandes de Lima e Silva, and Sandro Metrevelle Marcondes Lima e Silva. "A GTA welding cooling rate analysis on stainless steel and aluminum using inverse problems." *Applied Sciences* 7.2 (2017): 122.
[23] Huang, Yiming, et al. "An improved model of porosity formation during pulsed GTA welding of aluminum alloys." *Materials Science and Engineering: B* 238 (2018): 122-129.
[24] Wang, Xinxin, Yi Luo, and Ding Fan. "Investigation of heat transfer and fluid flow in high current GTA welding by a unified model." *International Journal of Thermal Sciences* 142 (2019): 20-29.
[25] Xu, Xinkun, et al. "Effect of distance between the heat sources on energy transfer behavior in keyhole during laser-GTA welding titanium alloy." *Journal of Manufacturing Processes* 55 (2020): 317-325.
[26] Shrivastava, Mayank, and Rajeev Kumar. "Optimization of GTA Welding Parameters for AISI 304 Stainless Steel using Taguchi Method." *Available at SSRN 3566687* (2020).
[27] Teng T.L and Lin C.C, "Effect of Welding Conditions on Residual Stresses Due to Butt Welds", International Journal of Pressure Vessels and Piping, Vol. 75, pp.857-864, 1998.